



Numerical investigation on the effectiveness of pile row in local sand trapping and beach protection

Xiaojian Liu^{1,3,4} · Peng Hou^{1,4} · Zihao Duan² · Chunhua Huang^{1,4} · Cheng Liu^{1,4} · Yong He^{1,4,5} · Huiqun Guo^{1,4} · Bin Wang^{1,4} · Shijun Wang^{1,4} · Qisong Wang^{1,4} · Xiaowei Zhu^{1,4} · Wancheng Yuan⁶ · Bingbing Zhao⁷

Received: 23 August 2021 / Accepted: 17 June 2022 / Published online: 6 July 2022
© Springer-Verlag GmbH Germany, part of Springer Nature 2022

Abstract

As novel coastal structures, pile row structures, such as breakwaters, have received increasing attention owing to their advantages in coastal protection and coastal landscape improvement. In this study, a nonlinear sediment model is developed based on OpenFOAM® to explore the effect of the pile row structure on the evolution of sandy beaches by waves. Its robustness was proved by published data related to two typical cases, that is, a pure sandy beach and a single pile on a sandy beach. Subsequently, the beach evolution and pile row with varied pile spaces S/D (the D is the pile diameter and S indicates the space between adjacent piles) on the beach were modeled. In addition, a long-term simulation was performed. The results revealed that the backrush-induced beach scour was larger than that induced by the uprush during wave propagation along sandy beaches. Sandy beach morphology changes because of the construction of the pile row structure by adjusting the wave motion, and local vortices and their evolution did not exhibit a simple linear relation following the variation in S/D . The local scour decreased with the increase in S/D when the S/D was less than 1.6, but it increased on the seaside of the piles and both side faces, except the leeside for S/D increased from 1.6 to 1.8. Meanwhile, in the nearshore zone, the pile row structure was effective in trapping beach sand, and its effectiveness was more remarkable as the S/D decreased. The findings would be useful in assessing the influence of pile row structures on beach evolution by waves and provide a basis for coastal protection engineering.

Keywords Pile row structure · Wave · Sandy beach evolution · Three-dimensional model

1 Introduction

The pile row structure, an active measure, was used to protect the coasts. In view of the relatively low cost and capability of both protecting the landscape and maintaining the coastal environmental quality, those in the form of pile-type

breakwaters are becoming increasingly popular in coastal areas (Jiang et al. 2019). An example of a pile row breakwater in Langkawi, Malaysia, can be found in Reedijk and Markus (Reedijk and Muttray 2007). Compared with common environments, extreme cases such as tsunami waves can result in disastrous potential destruction, including damage to beach erosion and structural failures of buildings (Mo

Responsible Editor: Zhiyu Liu

✉ Zihao Duan
duanzh.18b@igsnr.ac.cn

¹ Pearl River Hydraulic Research Institute, Pearl River Water Resources Commission of the Ministry of Water Resources, Guangzhou, Guangdong, China

² National Engineering Laboratory for Port Hydraulic Construction Technology, Tianjin Research Institute for Water Transport Engineering, M.O.T., Tianjin, China

³ Key Laboratory of Water-Sediment Sciences and Water Disaster Prevention of Hunan Province, Changsha, Hunan, China

⁴ Key Laboratory of the Pearl River Estuary Regulation and Protection of Ministry of Water Resources, Guangzhou, Guangdong, China

⁵ Southern Marine Science and Engineering Guangdong Laboratory, Zhuhai, China

⁶ China Harbour Engineering Company Limited, Beijing, China

⁷ China Railway Fifth Survey and Design Institute Group Co., Ltd., Beijing, China

et al. 2013). Such destructive disasters occurred in coastal areas during the American Samoa Tsunami on September 29, 2009 (Roeber et al. 2010), and the Japan Tsunami on March 11, 2011 (Mori and Takahashi 2012), leading to catastrophic life and economic losses (Fig. 1).

Historically, the instability of the foundation structure induced by extreme environments has been proven to be one of the damaging causes of coastal structures, which may further cause more casualties (Kuswandi et al. 2016; Tonkin et al. 2003; Saatcioglu et al. 2004; FEMA 2008; USGS 2010). Recently, the 2011 tsunami that struck Japan also caused deep scours around large coastal structures, as delineated by Takahashi et al. (Takahashi et al. 2011). They pointed out that scouring is the most typical failure of coastal structures. Apart from the aforementioned scour around coastal structures, Reedijk and Markus (Reedijk and Muttray 2007) discovered that pile rows are effective in trapping nearshore sand during the Indian tsunami event. However, owing to the lack of limited field information on local wave conditions and topography, this phenomenon could not be clearly clarified. Therefore, they recommended conducting further studies for pile rows, such as varying the pile row spacing to evaluate the effect on shoreline changes and to formulate reasonable design criteria for such structures. Physical and numerical experiments can simulate some interesting scenarios through effective control over critical factors, which are helpful in improving the understanding of these processes.

Numerous studies have been conducted on the local scour on pile structures under steady flows (Rambabu et al. 2003; Nielsen et al. 2013), steady waves (Sumer et al. 2007; Larsen et al. 2018), and the combination of steady flows and waves (Sumer and Fredsøe 2001; Qi and Gao 2014). It is worth mentioning that the pile structures were placed on a horizontal seabed in the aforementioned studies. In practical applications, many structures are constructed on sloping beaches, where extremely large wave forces are caused by wave breaking and high-speed roller run-up (Xiao and Huang 2014). These wave behaviors lead to substantial erosion and scour (Kato et al. 2001). Additionally, the scour mechanism induced by a tsunami bore, which is defined

as supercritical flow owing to its Froude number, which is much larger than one is different from a steady current and consistent wave field (Pan and Huang 2012). Kato et al. (Kato et al. 2001, 2000) and Tonkin et al. (Tonkin et al. 2003) conducted a series of large-scale physical experiments to examine scouring mechanisms induced by tsunami-like solitary waves around a cylinder on a sandy beach and discovered that the most rapid scour occurred at the end of the drawdown process after the flow velocity subsided. This contributed to a reduction in the effective wave stress on the sediment particles. Recently, Kuswandi et al. (Kuswandi et al. 2016) investigated erosion and deposition patterns around an onshore cylinder after a tsunami-like surge. The results revealed that compared to the final scour caused by sediment redeposition, the maximum depth of the local scour around a vertical cylinder was deeper during the tsunami attack, and the maximum local scour could reach approximately 0.60 of the tsunami height.

In view of the high cost and limited measurement capability employed in laboratory experiments and field observations, numerical simulations enable us to use an alternate approach to explore the scour mechanics of tsunami–wave interactions with pile structures. Pan and Huang (Pan and Huang 2012) performed a numerical simulation of the experiment in Tonkin et al. (Tonkin et al. 2003) using the linked 2D hydrodynamic and sediment scour model and found that the simulation reproduced the experimental results well, except for the short-term bottom profile near the maximum scour. Practically, the interaction of the wave-pile structures-sandy beach is highly nonlinear and local, but strong turbulence exists near the seabed and the free surface. However, the aforementioned models driven by shallow water equations do not consider these factors. Kuswandi et al. (Kuswandi et al. 2017) simulated the three-dimensional (3D) flow pattern of a tsunami surge around a cylinder pile using DualSphysics software. They pointed out that the local maximum scour around the cylinder occurred along both sides, whereas the front and rear scours were not completely developed. To the best of our knowledge, the aforementioned studies have primarily focused on the case of a cylinder on a beach slope, and the arrangement in a row of piles was not considered. However, the influence of the interference between adjacent piles on hydrodynamic and sediment transport

Fig. 1 Pile row breakwater in Langkawi. The left figure is the front view of the southern pile row in the beach of the Pelangi Beach Resort in 1998; the right figure is the side view. (Reprinted from “Pile row breakwaters at Langkawi, Malaysia, 10 years of beach development” (Reedijk and Muttray 2007))



cannot be ignored (Roeber et al. 2010), and the corresponding scour mechanisms of this process are still not well understood.

To improve the understanding of the aforementioned problems, a 3D numerical model was developed to analyze the effects of piles on hydrodynamic and sediment transport based on Open Field Operation and Manipulation (OpenFOAM). OpenFOAM has been effectively applied to simulate wave dynamics using an interFoam solver combined with the boundary conditions of wave generation and absorption, such as waves2Foam (Jacobsen et al. 2012) and IH-FOAM (Higuera et al. 2013). Accordingly, we developed the sediment transport and bed morphological change module in OpenFOAM owing to unavailability in the official version. Moreover, the local flow field of pile row breakwater is typically simulated by LES turbulence model, primarily because it is difficult to model the violent jet and flow separation in the slots of the piles using the RANS turbulence model (Yao et al. 2018). However, for sediment motion, the stochastic nature of the flow reflects nonlinearly onto the bed change and results in larger spatial gradients when using the LES turbulence model, and the allowable calculation stability will be lowered considerably. Therefore, the RANS turbulence model was considered in this study because it is preferable to predict seabed scour than the LES turbulence model (Liang et al. 2005; Jacobsen and Fredsøe 2011).

To achieve our objectives, this study had the following primary objectives. Mathematical methods, including hydrodynamic and sediment controlling equations, boundary conditions, and numerical schemes, are introduced in Section 2. Model validations of the free surface elevation, velocity, and sandy beach scour are presented to demonstrate the robustness of this self-extended model in Section 3. A detailed analysis of the sandy beach change without the pile structure, as well as the three-dimensional vortex structure, bed shear stress, and beach scour with the pile structure, is described in Section 4. The effect of pile-row breakwaters on beach evolution is discussed in Section 5. Finally, a summary of the study is presented in Section 5.

2 Mathematical model

2.1 Hydrodynamic model

The RANS equations were employed to model unsteady and incompressible flows, and the continuity and momentum equations are as follows:

$$\nabla \cdot \mathbf{u} = 0 \tag{1}$$

$$\frac{\partial \rho \mathbf{u}}{\partial t} + \nabla \cdot [\rho \mathbf{u} \mathbf{u}^T] = -\nabla p + \rho \mathbf{g} + \nabla \cdot [\mu \nabla \mathbf{u} + \rho \boldsymbol{\tau}^*] + \sigma_T \kappa_\gamma \nabla \gamma \tag{2}$$

where $\mathbf{x} = (x_i, x_j, x_k)$ indicates the Cartesian coordinate system and $\mathbf{u} = (u_i, u_j, u_k)$ indicates the velocity vector under

this coordinate system. ρ denotes the density of the fluid, ρ^* represents the pressure exceeding the hydrostatic pressure, and g represents the acceleration due to gravity. The $\sigma_T \kappa_\gamma \nabla \gamma$ represents the surface tension term, where σ_T and κ_γ denote the surface tension coefficient and surface curvature, respectively; γ is the proportional field with tracking fluid motion. $\boldsymbol{\tau}^*$ denotes the turbulence stress tensor, which is expressed as

$$\boldsymbol{\tau}^* = \frac{2}{\rho} \mu \mathbf{S} - \frac{2}{3} k \mathbf{I} \tag{3}$$

where μ is the eddy viscosity, $\mathbf{S} = (\nabla \mathbf{u} + (\nabla \mathbf{u})^T)/2$ is the strain-rate tensor, and k is the turbulent flow energy. \mathbf{I} is the Kronecker delta function, where \mathbf{I} is equal to 1 if $i=j$, otherwise 0.

To close the RANS equations in this study, the $k - \epsilon$ turbulent model with a second-order term was employed, as follows:

$$k = \frac{1}{2} \overline{\mathbf{u} \cdot \mathbf{u}^T} \tag{4}$$

$$\epsilon = \frac{C_\mu^{0.75} k^{1.5}}{l} \tag{5}$$

where ϵ indicates the rate of turbulent dissipation, C_μ represents a dimensionless coefficient specified as 0.09, and l denotes the turbulence length scale.

The k and ϵ is described as follows, respectively.

$$\frac{\partial k}{\partial t} + \nabla(k\mathbf{u}) = \nabla \left(\frac{\nu_t}{\sigma_k} \nabla k \right) + 2 \frac{\nu_t}{\rho} |\nabla \mathbf{u}|^2 - \epsilon \tag{6}$$

$$\frac{\partial \epsilon}{\partial t} + \nabla(\epsilon \mathbf{u}) = \nabla \left(\frac{\nu_t}{\sigma_\epsilon} \nabla \epsilon \right) + 2 C_{1\epsilon} \nu_t |\nabla \mathbf{u}|^2 \frac{\epsilon}{k} - C_{2\epsilon} \frac{\epsilon^2}{k} \tag{7}$$

where ν_t is the turbulence kinematic viscosity coefficient and $C_{1\epsilon}, C_{2\epsilon}, \sigma_k,$ and σ_ϵ represent empirical coefficients of 1.44, 1.92, 1, and 1.3 in the present study.

Furthermore, the free surface was simulated using the modified VOF method, which is defined as

$$\frac{\partial \alpha}{\partial t} + \nabla \cdot \mathbf{u} \alpha + \nabla \cdot \mathbf{u}_r \alpha (1 - \alpha) = 0 \tag{8}$$

where each phase of air and water is represented by the volume fraction (α), varying from 0 (air) to 1 (water). When compared with the traditional VOF method, the last term of Eq. (8) introduces an additional compression term (u_r is the relative velocity) to control excessive diffusion and smearing of the interface (Jacobsen et al. 2012).

Bed shear stress is a fundamental parameter that connects hydrodynamic characteristics to sediment transport. Some formulas, such as the wall function method (Babaeyan-Koopaei et al. 2002), friction-based method (Schlichting

1979), turbulent viscosity-based method (Zeng et al. 2005), and turbulent kinetic energy-based method (Galperin et al. 1988), have been introduced to estimate bed shear stress. In this study, the method proposed by Arzani et al. (Arzani et al. 2016) was employed, and the detailed configurations are as follows.

$$\tau = \tau_t - (\tau_t \cdot \mathbf{n})\mathbf{n} \quad (9)$$

where τ_t indicates the wall traction force expressed as $\sigma \cdot \mathbf{n}$, \mathbf{n} is the unit normal vector perpendicular to the surface, and σ is the stress tensor calculated by

$$\sigma = -p\mathbf{I} + 2\mu\mathbf{S} \quad (10)$$

where p denotes the pressure in the pressure-induced stress term of $-p\mathbf{I}$ and $2\mu\mathbf{S}$ is the viscous stress term, which is determined by the bottom fluid movement.

2.2 Morphodynamic model

Accurate modeling of the evolution of sandy beaches requires consideration of multiple mechanisms of sediment transport and erosion. The details of each component of the sediment modules in this study are described below. To better capture the bed load transport process, we adopted the formula proposed by Engelund and Fredsøe (Engelund and Fredsøe 1976). This formula has been rigorously verified to solve the question of sandy beach evolution in published studies (Engelund and Fredsøe 1976; Allen 1982).

$$q_b = \begin{cases} 18.74(\theta - \theta_c)(\theta^{0.5} - \theta_c^{0.5})\sqrt{Rgd_{50}}d_{50} & \text{if } \theta > \theta_c \\ 0 & \text{if } \theta < \theta_c \end{cases} \quad (11)$$

$$\theta = \frac{\tau}{\rho g R d_{50}} \quad (12)$$

$$R = \frac{\rho_{sed} - \rho}{\rho} \quad (13)$$

where q_b denotes the bed load transport across a unit width, d_{50} indicates the median sand diameter, R indicates the relative sediment density, θ symbolizes the Shields number, and the critical Shields number of θ_c is different owing to different bed slopes; thus, we have updated it referring to the research of Allen (Allen 1982).

$$\frac{\theta_c}{\theta_{co}} = \cos\beta + \frac{\sin\beta}{\tan\varphi} \quad (14)$$

It can be observed from Eq. (14), the value of θ_c decreases (i.e., negative slope) when the sediment moves downward along the slope and the value of θ_c increases (i.e., positive angle) when the sediment moves upward along the slope. Here, φ denotes the angle of repose of the sediment. θ_{co}

indicates the critical Shields parameter for a flat sand bed, which is given (Soulsby and Whitehouse 1997) by

$$\theta_{co} = \frac{0.3}{1 + 1.2D_*} + 0.055[1 - \exp(-0.02D_*)] \quad (15)$$

D_* is dimensionless sand size

$$D_* = \left[\frac{gR}{v^2}\right]^{1/3} d_{50} \quad (16)$$

The rates of bed load transport in different directions are calculated by

$$q_{bi} = q_b \frac{\tau_i}{|\tau|} - C|q_b| \frac{\partial\eta}{\partial x_i} \quad (17)$$

where η indicates the bed surface elevation and C denotes a constant parameter varying from 1.5 to 2.3, which could characterize the influence of the bed slope on the sediment flux. In this study, C was set to 1.5, as per to Brørs (Brørs 1999) and Liu and García (Liu and García 2008).

Generally, the suspended sediment transport process can be expressed by the classical convection–diffusion equation, as follows:

$$\frac{\partial c}{\partial t} + \nabla \cdot (\mathbf{u} + w_s \frac{\mathbf{g}}{|\mathbf{g}|})c = \nabla \cdot (\frac{v_d}{\sigma_c} \nabla c) \quad (18)$$

where c denotes the concentration of suspended sediment, v_d corresponds to the diffusivity coefficient of the sediment, σ_c is the turbulent Schmidt number, and w_s indicates the fall velocity of the sediment that could be influenced by different particle concentrations.

$$w_s = (1 - c)^\zeta w_{s0} \quad (19)$$

where ζ indicates a constant and w_{s0} represents the settling velocity in clear water given (Allen 1982) by

$$w_{s0} = \frac{v}{d_{50}} [(10.36^2 + 1.049D_*^3)^{1/2} - 10.36] \quad (20)$$

In fact, there were clear interaction processes in the shallow water zone. To ensure that the sediment drops out immediately when accidentally left in the air phase, an additional volume fraction α term was introduced in Eq. (18) as follows:

$$\frac{\partial c}{\partial t} + \nabla \cdot (\alpha\mathbf{u} + w_s \frac{\mathbf{g}}{|\mathbf{g}|})c = \nabla \cdot (\alpha \frac{v + v_d}{\sigma_c} \nabla c) \quad (21)$$

where the velocity term is multiplied by α . Additionally, v in Eq. (21) was used to maintain the stability of the numerical model. If v_d is zero, numerical instability occurs. Therefore, v guarantees an effective solution for the advection–diffusion problem and avoids the occurrence of the convection problem, which is more difficult to solve in the numerical model (Leveque 2002).

The Exner equation was adopted to model the bed elevation change by solving the sediment continuity:

$$\frac{\partial z}{\partial t} = \frac{1}{1-n}(-\nabla q_b + D - E) \tag{22}$$

where n indicates beach porosity; the deposition rate D is given by

$$D = c_s w_s \tag{23}$$

where c_s represents the bed surface’s sediment concentration.

The sediment concentration at a reference height Δ_b above the bed can be calculated using the following formula:

$$c_b = \frac{0.015 d_{50} T^{1.5}}{\Delta_b D_*^{0.3}} \tag{24}$$

in which T indicates the non-dimensional excess shear stress,

$$T = \left(\frac{\mu_{sc} \tau}{\tau_{cr}} - 1\right)^{1.5} \tag{25}$$

where μ_{sc} indicates the effective shear stress coefficient and τ_{cr} denotes critical shear stress.

The E in the Eq. (22) represents the entrainment rate calculated by van Rijn (Rijn 1984):

$$E = \frac{v + v_t}{\sigma_c} \cdot \nabla c \tag{26}$$

Finally, the computational mesh is moved such that the bottom mesh is conformal to the sediment bed to realize model coupling between hydrodynamic and morphological dynamics. The mesh movement primarily adopted the method proposed by Jasak and Tuković (Jasak and Tukovic 2006). Meanwhile, an additional mass conservative sand slide algorithm proposed by Khosronejad et al. (Khosronejad et al. 2011) was utilized to maintain the bed slopes so as not to exceed the repose angle of the sediment. The Exner equation at both points P and its i th neighbor is given by:

$$\frac{(z_{bp} + \Delta z_{bp}) - (z_{bi} + \Delta z_{bi})}{\Delta l_{pi}} = \tan\phi \tag{27}$$

where z_{bp} denotes the bed elevation at point P , z_{bi} indicates the bed elevation at the i -th neighbor, Δl_{pi} signifies the horizontal distance between two cell centers, and Δz_{bp} and Δz_{bi} symbolize the corresponding corrections imposed to satisfy the repose angle of the sediment. By balancing the cell mass, Δz_{bp} and Δz_{bi} can be expressed as

$$A_{bp} \cdot \Delta z_{bp} - \sum_i A_{bi} \cdot \Delta z_{bi} = 0 \tag{28}$$

where A_{bp} indicates the projection of the bed cell P and A_{bi} is the projection of its i th neighbor.

2.3 Boundary conditions

Boundary conditions are central for reproducing the physical experimental process. In the proposed numerical model, the active wave-absorbing boundary was applied at the inlet and outlet of the model, which was developed by Higuera et al. (Higuera et al. 2013). Compared with the approach given by Jacobsen et al. (Jacobsen et al. 2012), this approach reduces the computational domain because no relaxation region is required. Additionally, the expressions proposed by Lee et al. (Lee et al. 1982) were applied to describe the free surface and velocity of the inlet boundary:

$$\eta = H \operatorname{sech}^2\left[\sqrt{\frac{3H}{4h^3}}X\right] \tag{29}$$

$$\frac{u}{\sqrt{gh}} = \frac{\eta}{h}\left[1 - \frac{1}{4}\frac{\eta}{h} + \frac{h}{3}\frac{h}{\eta}\left(1 - \frac{3}{2}\frac{z^2}{h^2}\right)\frac{d^2\eta}{dX^2}\right] \tag{30}$$

$$\frac{w}{\sqrt{gh}} = \frac{-z}{h}\left[\left(1 - \frac{1}{2}\frac{\eta}{h}\right)\frac{d\eta}{dX} + \frac{1}{3}h^2\left(1 - \frac{1}{2}\frac{z^2}{h^2}\right)\frac{d^3\eta}{dX^3}\right] \tag{31}$$

where η denotes the wave free surface elevation, H indicates the wave height, h denotes the water depth, $X = x - ct$, $c = \sqrt{g(h + H)}$ indicates the wave propagation velocity, and u and w denote the velocities along the flow direction and vertical direction, respectively.

The other boundary conditions are as follows: The no-slip condition was applied to the surface between the sand layer and pile (Lee et al. 1982), in which the y Plus value was approximately 10 mm, the first layer of the mesh was approximately 0.2 mm, and the normal pressure gradient was zero. The top boundary is the atmospheric interface, and the total pressure is zero in the atmospheric interface. The vertical movement speed of the sandy-bed boundary was consistent with the changing speed of the sandy-bed elevation. Moreover, a symmetrical boundary condition was adopted on both sides of the domain to improve the computational efficiency, allowing for the symmetrical distribution of the domain along the flow direction. Regarding the numerical model grid resolution, from the inlet of the domain to the fore-slope toe, the grid size decreased gradually from 20 to 4 mm (see Supplementary Fig. 1). The core region, starting from the still water level to the outlet, maintained a constant smaller cell size (0.2 mm) to capture the breaking wave-induced run-up. A finer mesh reduced to 0.2 mm was employed around the surfaces of the piles.

2.4 Numerical schemes

The Euler scheme was employed to solve the time derivative, and the finite-volume method was utilized to discretize

the 3D computational space. The pressure–velocity solver used the PIMPLE algorithm that combined the pressure implicit, operator split (PISO), and pressure link equation semi-implicit (SIMPLE) methods. Meanwhile, the multi-dimensional universal explicit solution limiter (MULES) scheme was employed to maintain the boundedness of the volume fraction. The gradient term and Laplacian term were solved using the Gaussian linear scheme and Gaussian linear modified scheme, respectively.

In addition, different sediment forms were addressed separately. First, the bed load transport process was solved using the shear stress with the hydrodynamic model. The suspended sediment was then transported passively based on the convection–diffusion equation. Once sediment transport was addressed, the Exner equation was employed to solve the beach profile change. Generally, the beach morphology change occurs in a 3D space, whereas the Exner equation is a two-dimensional (2D) equation. This process of flow information mapping from 3D space to 2D space was solved using the finite area method (FAM). The details can be found in the OpenFOAM® user guide.

3 Model validation

3.1 The beach profile change without the presence of structure

To ensure the transport capacity of the water and sediment in our model, we first calibrated the model using the experimental data of Kobayashi and Lawrence (Kobayashi and Lawrence 2004). The beach with a slope of 1:12 was applied by sediment with grain size of 0.18 mm and porosity of 0.4. The experimental setup is presented in Fig. 2, where wave gauges were employed to capture the wave elevation change along the wave flume, in which G1 was placed at the toe of the slope to

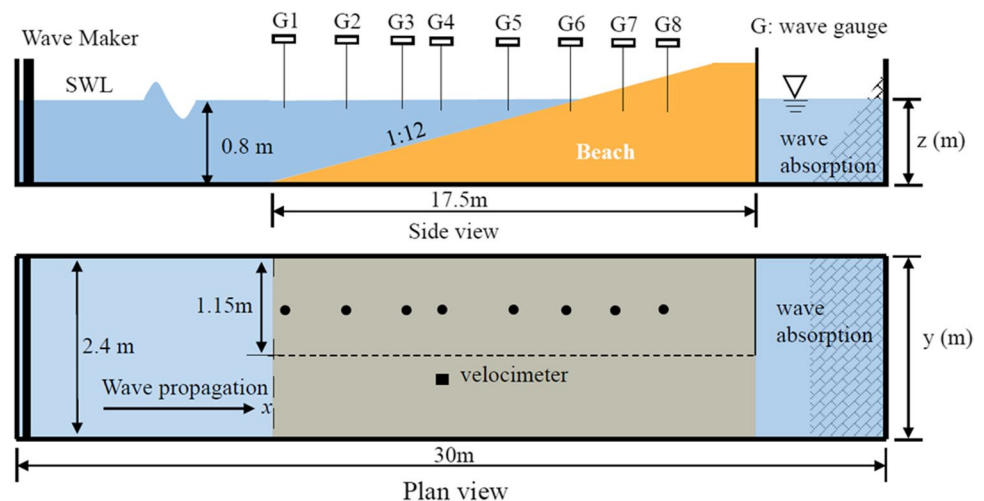
measure the incident solitary wave, G2–G5 were utilized to measure the solitary wave shoaling and breaking, and G6–G8 were used to measure the breaking wave run-up and rundown in the swash zone. The velocity was measured using a velocimeter installed at the location 13.5 cm from the flume centerline at the cross-shore location of G3 and 6 cm above the bed surface. The initial wave height was 21.6 cm, and the wave propagated on the beach at a water depth of 80 cm. When the water surface became stable after the action of the first solitary wave, the second solitary wave began traveling toward the beach with the same wave height as the first solitary wave, and the cycle was repeated. The beach profile and hydrodynamic changes were measured at the end of the fourth wave.

Figure 3 shows the numerical and experimental wave surface elevations, streamwise velocity, and beach profile changes obtained through the model simulation. We found that the simulated results agreed well with the experimental results, particularly for the wave height and velocity. However, the simulated value of the beach near the coastline (approximately at $x = 10$ m) was higher than the measured value, which could be attributed to the overestimation of turbulent dissipation and some underestimation of the current velocity induced by the backwash. Nevertheless, in this study, the self-developed coupled model could reasonably simulate reproduced wave propagation and the associated beach profile changes.

3.2 The beach evolution with the presence of monopile

A physical experiment of a solitary wave producing scour around a pile conducted by Tonkin et al. (Tonkin et al. 2003) was used to validate the sediment transport capacity in the presence of a pile structure. The sandy beach was constructed with a constant slope of 1:20, where the sediment median diameter was 0.35 mm and density was 2643 kg/m^3 . The water

Fig. 2 Side view (top) and plan view (bottom) of experimental setup of solitary wave propagation along the sandy beach (adapted from “Cross-shore sediment transport under breaking solitary waves” (Kobayashi and Lawrence 2004))



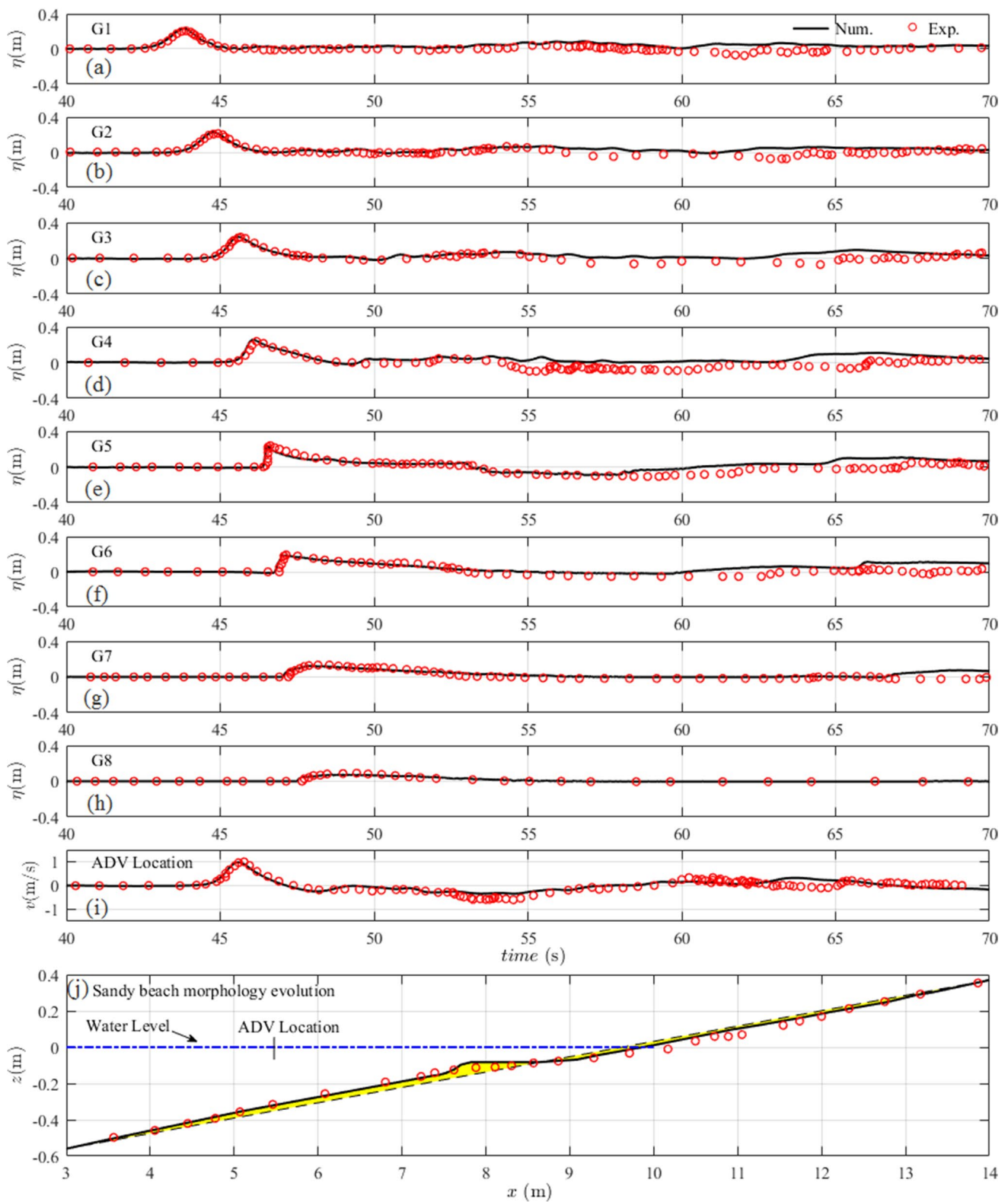


Fig. 3 Comparison between the simulated and experimental results for the wave surface elevations, streamwise velocity, and beach profile (ADV is the acoustic Doppler velocimeters). The red cycle represents the experimental data. The solid line denotes the wave height of the numerical data in Fig. 3(a)–(i) and the sandy

beach morphology evolution of the numerical data in Fig. 3(j). In Fig. 3j, the dash line corresponds to the original sandy beach, and the dotted line is the water level. (Adapted from “3D modeling and mechanism analysis of breaking wave-induced seabed scour around monopile” (Liu et al. 2020).)

depth and wave height were 2.45 m and 0.22 m, respectively. A pile with a diameter of 0.5 m, as shown in Fig. 4, was placed at the coastline. Several measurement instruments were arranged to capture the water and sediment motion, in which the wave surface in a typical location (A, C, D) was measured using a wave gauge and the flow velocity at station B was measured using an electromagnetic flowmeter located at 2.525 m above the bed surface. The bed change at three locations, that is, C, D, and E, around the monopile was recorded using a digital camera. Detailed information regarding this experiment can be found in Tonkin et al. (Tonkin et al. 2003).

Figure 5 shows the numerical and experimental wave surface elevation, streamwise velocity, and beach change around the monopile through the model simulation, in which satisfactory agreement could be found for the hydrodynamic parameters at all locations except for the velocity at station B, since $t=13$ s. This is because of the shallow water depth during the wave drawdown that the electromagnetic flowmeter cannot measure the flow velocity. The beach scour in terms of around the monopile (i.e., the seaside point C, leeside point D, and side point E) was captured using a numerical model, which was consistent with the physical result in the variation trends and magnitude. We also found that the numerical maximum scour depth was slightly smaller than the physical result, which resulted from the beach seepage flow phenomenon observed by Tonkin et al. (Tonkin et al. 2003). However, this cannot be simulated using the proposed model.

Overall, this self-developed model can not only simulate the propagation of breaking waves on sandy beaches, but also the wave interaction with the pile structure on the sandy beach. Based on this model, we developed several scenarios to explore the effect of pile row breakwaters on beach evolution. The model scenario configuration, scouring monitoring probes, and monitoring profiles can be found in Fig. 6. In this study, the ratio of center space between piles to pile diameter ($S/D=1.2, 1.4, 1.6, 1.8$, the pile diameter D is 0.5 m and S indicates the space between adjacent piles) was changed, while other factors were

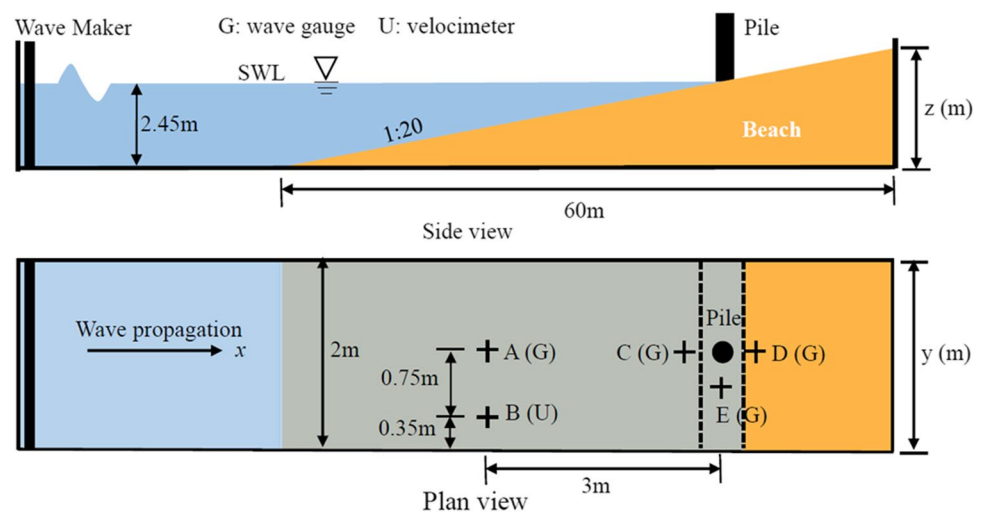
kept unchanged. The constant parameters are as follows: the water depth h is 2 m, wave height H is 0.6 m, beach slope m is 1:20, and the horizontal distance between the slope toe and offshore pile model is 3 m. In addition, following the aforementioned water–sediment parameters, an additional scenario without the presence of a pile structure on the beach was modeled.

4 Results and discussions

4.1 Beach profile evolution by wave action

Figure 7 shows the wave surface, suspended sediment, and beach profile changes during the wave propagation along the sandy beach. During the wave run-up, the incident wave became steepened and skewed toward the beach, and the wave broke as a plunging breaker owing to wave shoaling on the slope. Subsequently, the breaking waves immediately injected fluid with air entrainment on the free surface. However, no remarkable sediment suspension was observed. As the wave moved onshore, the breaking wave-induced bore picked up amounts of sediment from the sandy beach into suspension, but the beach had not been obviously eroded, which could be due to the fact that the wave direction was inconsistent with the sediment gravity and bottom friction. During the wave drawdown, a hydraulic jump formed by retreating the water tongue collided with the offshore still water and then evolved into a turbulent flow roll. Meanwhile, sediment transport was obvious by high-speed sheet-flow and induced remarkable offshore net deposition and onshore net erosion near the location of the hydraulic jump. Lastly, the sea was calm when the backrush energy was insufficient to sustain the hydraulic jump. The above sandy beach evolution is consistent with the physical experimental results of Kobayashi and Lawrence (Kobayashi and Lawrence 2004).

Fig. 4 Experiment setup of solitary wave interaction with a vertical pile in a sandy beach (adapted from “Tsunami scour around a cylinder” (Tonkin et al. 2003))



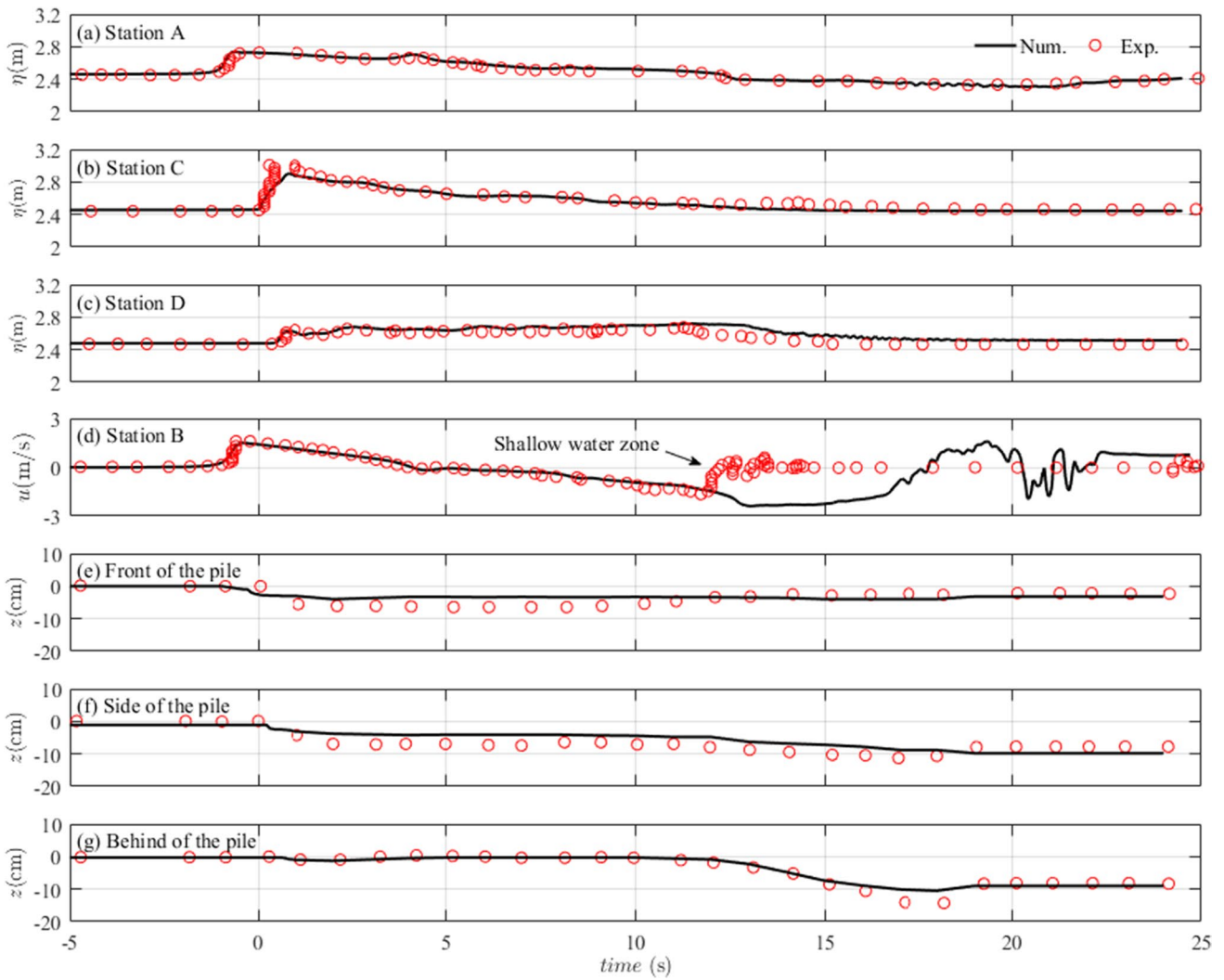
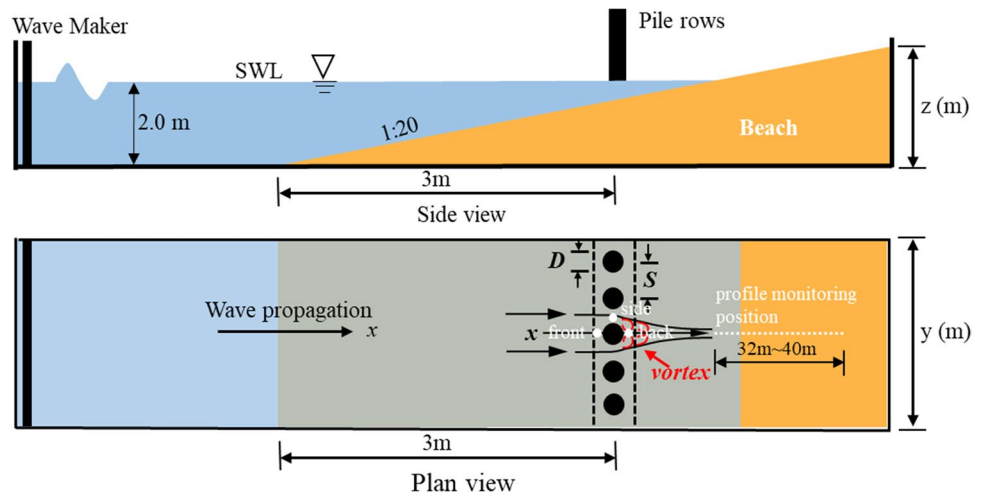


Fig. 5 Comparison between the simulated and experimental results for the wave surface elevations, streamwise velocity, and seabed scour ((a)–(c) are the wave height in locations of the station A, C, and D,

respectively. (d) is the flow velocity in the location of the station B. (e)–(g) are the wave height around the pile, respectively.)

Fig. 6 Model setup of wave interaction with pile row in a sandy beach



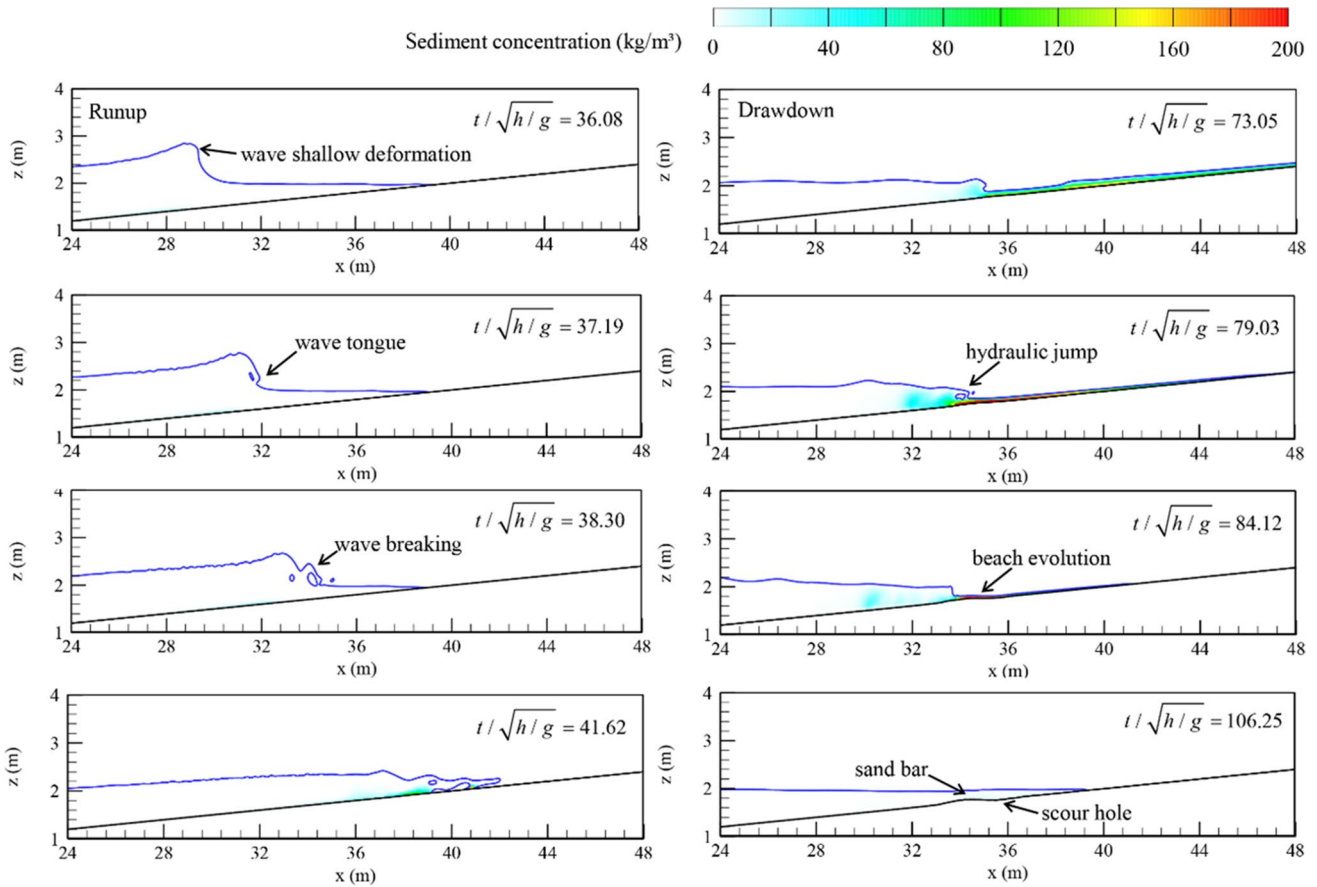


Fig. 7 Wave surface, suspended sediment, and beach profile changes during the wave propagation along the sandy beach

4.2 Vortex structure around pile row

The flow blockage induced by the interference between adjacent piles enhances hydrodynamic complexity (Roerber et al. 2010), thereby affecting nearshore sediment transport. Typically, this interaction is accompanied by a certain law of turbulence-ordered movement, that is, a quasi-ordered structure, which is often described by the deformation, stretching, and breaking characteristics of three-dimensional vortices (Baykal et al. 2017). In this study, the Q criteria method (Jeong and Hussain 1995), which is a quadratic invariant of the velocity gradient tensor, was employed to illustrate the motion of a large-scale vortex structure in turbulence, defined as

$$Q = \frac{1}{2} (|\Omega_{ij}| - |S_{ij}|) \tag{32}$$

where the Ω_{ij} and S_{ij} denote the vorticity and the rate of strain tensor,

$$\Omega_{ij} = \frac{1}{2} \left(\frac{\partial u_i}{\partial x_j} - \frac{\partial u_j}{\partial x_i} \right) \tag{33}$$

$$S_{ij} = \frac{1}{2} \left(\frac{\partial u_i}{\partial x_j} + \frac{\partial u_j}{\partial x_i} \right) \tag{34}$$

In particular, Q indicates the extent to which the vorticity is greater than the strain-rate tensor. If Q is greater than zero, it indicates that the vortex structure dominates in that region.

Figure 8 shows the variations in the vortex structure of a typical case (i.e., $h = 2$ m, $H = 0.6$ m, $m = 1:20$, $S/D = 1.6$), where the isosurface was displayed by $Q = 1 \text{ s}^{-1}$. We found that a horseshoe-shaped vortex structure formed around the foundation of the pile structure before the wave crest impacted the piles (e.g., $t/\sqrt{h/g} = 36.08$), where the vortices in the frontal zone were not obvious compared with those in the lateral zone. This is attributed to the adverse pressure gradient induced by the blocking of the structure and high-speed shear flow on the surface of the structure. During the impacting process (e.g., $t/\sqrt{h/g} = 36.63$), the horseshoe structure (see Supplementary Fig. 2) was elongated in the z direction following the wave run-up along the pile surface; however, it did not exhibit significant changes in the x and y directions. Subsequently (e.g., $t/\sqrt{h/g} = 40.51$), the reflected and transmitted waves are separated in the vicinity of the piles and

form a sequence of large-scale vortices, impacting the sandy beach. The stretched tail vortex gradually broke when the wave further ran up along the beach (e.g., $t/\sqrt{h/g} = 43.17$). Compared with the run-up process, it was found that the deformation of the vortices in front of the piles was extremely remarkable during drawdown (e.g., $t/\sqrt{h/g} = 81.90$). Meanwhile, a notable velocity gradient appeared because the velocity near the wave surface was higher than that near the bed. When the backflow continually moved seaward (e.g., $t/\sqrt{h/g} = 85.67$), the three-dimensional vortex structure was elongated and twisted until the wave energy could not support its development. Ultimately, the vortex structure broke around the piles (e.g., $t/\sqrt{h/g} = 87.05$), in which one part was directly dissipated on the bed, and another part was separated into numerous small vortices, which then disappeared offshore (e.g., $t/\sqrt{h/g} = 93.86$). Moreover, we also found that the influence scope of the vortices during run-up was less than that during drawdown.

The difference in the space between adjacent piles also affects vortex shedding near the piles. Figure 9 shows the variations in vortex shedding with pile space at two typical moments of $t/\sqrt{h/g} = 40.51$ and $t/\sqrt{h/g} = 87.05$. It was found that the flow blockage was enhanced as the pile space decreased during the run-up and generated a larger jet flow that impacted the beach. However, during drawdown, vortex shedding on the seaside of the pile row exhibited an opposite trend. This was attributed to the smaller pile spaces, which reduced the transmission of incident waves during the run-up, thereby resulting in a short duration of vortex shedding in front of the piles.

4.3 Effect of pile row to beach evolution

To discover the sediment transport and seabed scour around the pile row on a sandy beach and the effect of different pile spaces, the later moments of wave run-up and drawdown are shown in Fig. 10. It can be observed that the bed changes induced by sediment transport were more notable with a decrease in pile spaces during wave run-up. In particular, for the smaller pile space, that is, $S/D = 1.2$, there was an obvious cross characteristic of seabed scouring and infilling around the piles affected by the irregular vortex motion. During the wave drawdown, the scour depth on the seaside of the piles increased rapidly and extended further upstream; however, it did not exhibit a declining tendency with the increase in pile spaces, such as for the cases from $S/D = 1.6$ to $S/D = 1.8$. The final scouring depth around the piles for $S/D = 1.8$ was larger than that for $S/D = 1.6$, which could be related to the backwash, and it induced shear stress, as shown in Fig. 9 and Supplementary Fig. 3, respectively.

The scouring process and maximum scouring depth at the front, side, and back of the most centered pile in a row of piles (probe position is shown in Fig. 6) are shown in the left and right panels of Fig. 11, respectively. It can be observed that the bed was sharply scoured during the wave interaction with the piles and that the scouring depth at both sides was larger than the front and rear scours. The high-speed shear flow between adjacent piles induced a strong bottom shear stress, which resulted in considerable downcutting of the seabed, and this phenomenon was more obvious for smaller pile spaces (e.g., $S/D = 1.2$). Subsequently, the scouring depth also increased

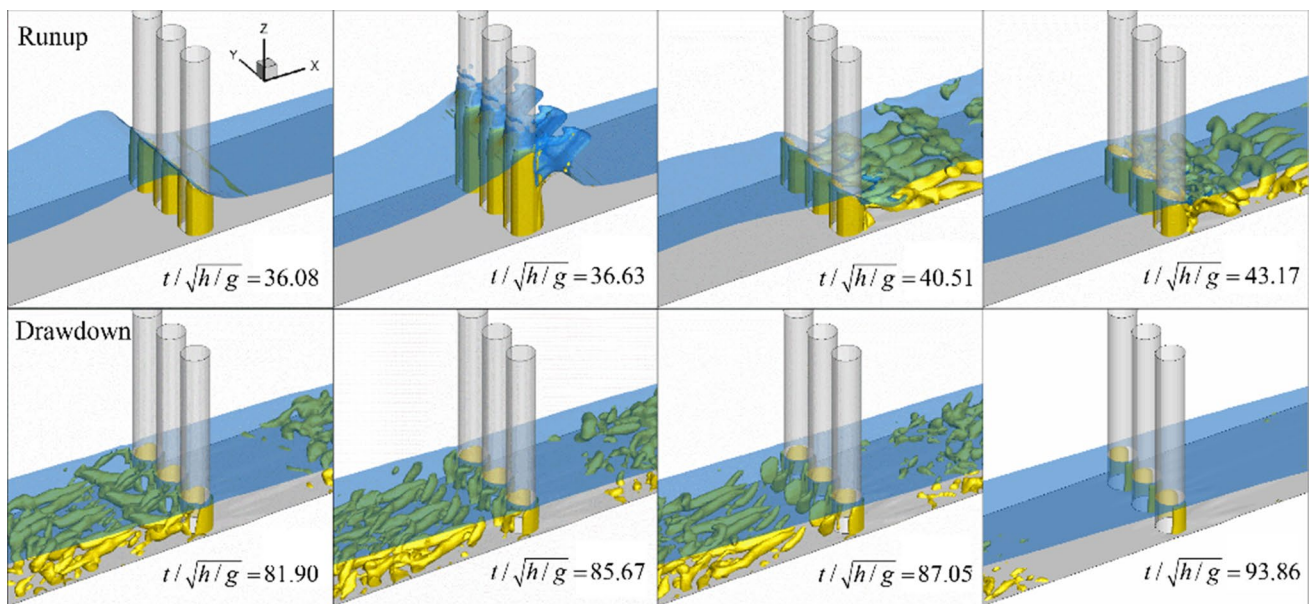


Fig. 8 Time series of the vortex structure ($Q = 1 \text{ s}^{-1}$. The blue color represents the water surface changes, and the yellow color represents the turbulent structures.)

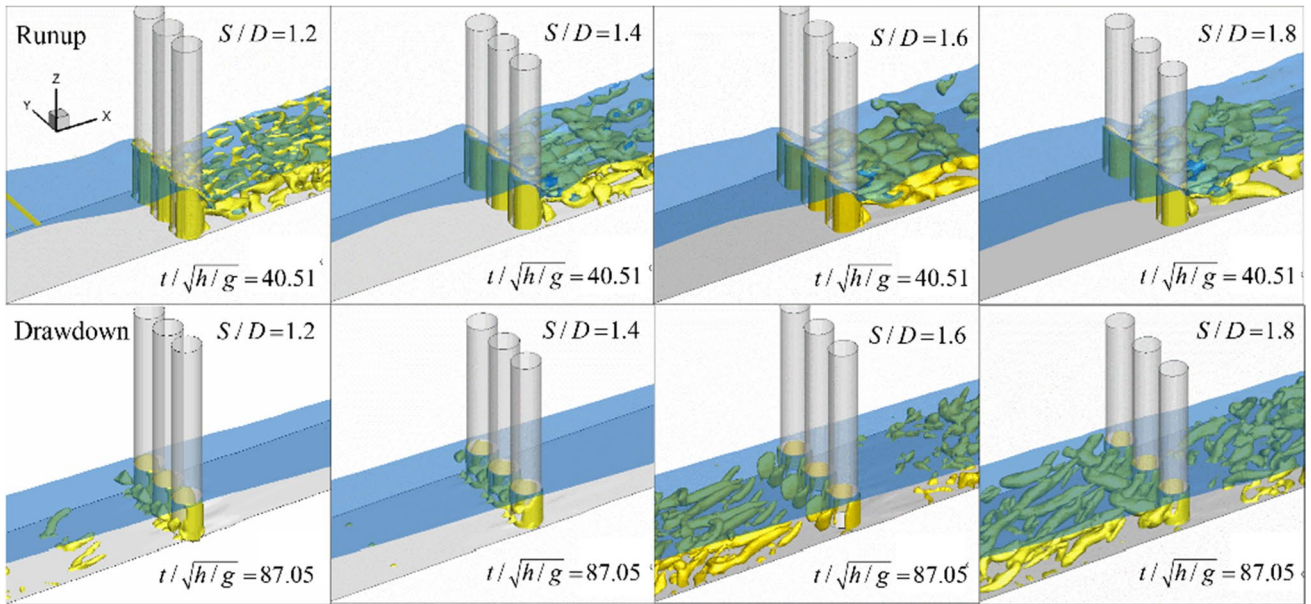
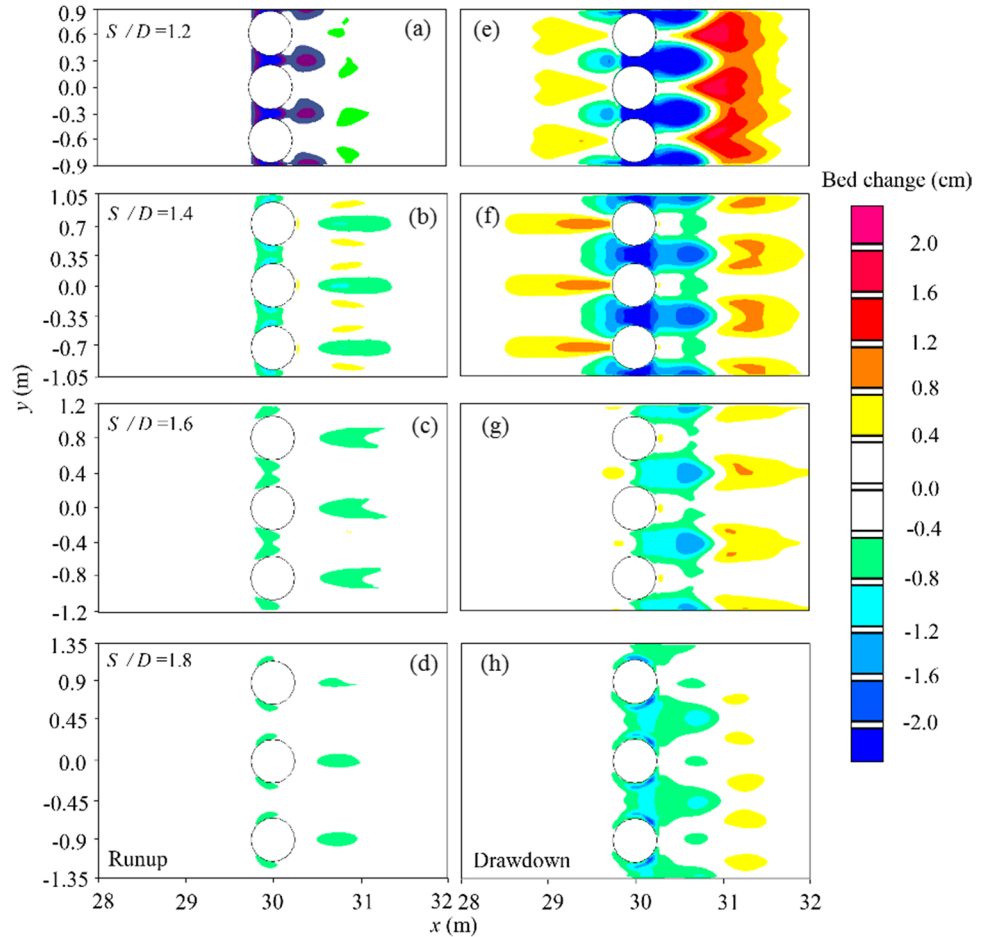


Fig. 9 Variations of the vortex structure with pile spaces ($Q = 1 \text{ s}^{-1}$. The blue color represents the water surface changes, and the yellow color represents the turbulent structures.)

Fig. 10 Variations of local scour morphology around the piles with pile spaces ((a)–(d) are local scour morphology changes in the process of the wave run-up under different S/D , respectively. (e)–(h) are local scour morphology changes in the process of the wave draw-down with corresponding S/D , respectively.)



because of sediment erosion by the reversed currents; however, the seabed at the back of the piles did not experience serious scouring compared with that at the front and side of the piles. Additionally, we also found that the maximum scouring depth exhibited an upward tendency as the pile spaces decreased at the three typical locations, particularly for the rear. The scouring depth reduction at the front and two sides from $S/D=1.6$ to $S/D=1.8$ can be attributed to the following two aspects. First, the seabed evolution did not show obvious differences between $S/D=1.6$ and $S/D=1.8$, according to the scouring morphology around the piles (Fig. 10) and time series of scouring depth (left panel of Fig. 11). This indicates that the hydrodynamic characteristics caused by the blocking of the piles share some similarities between the two scenarios. Second, the wave transmission increased from $S/D=1.6$ to $S/D=1.8$; thus, the intense reversed currents could lead to obvious net erosion in the nearshore region of the piles, which was proved by the sediment degradation direction shown in the right panel of Fig. 11.

Besides inducing local scour around the piles, waves affect nearshore beach evolution. Figures 12a and b show the nearshore beach profile changes (profile position is shown in Fig. 6) and the maximum scour depth. The scouring scope of sandy beaches increased with increasing space between piles, and a larger pile space induced a larger seabed change. This demonstrates that a

smaller distance between adjacent piles leads to smaller wave transmission because of the enhanced flow blockage effect, which then dissipates additional wave energy, correspondingly decreasing the impact on the sandy beach.

Subsequently, comparisons of nearshore beach evolution without and with piles on the beach are shown in Fig. 13. The sand bar and scour hole moved landward under the effect of a row of piles, and the scope of the beach profile change decreased to some extent. Furthermore, the smaller pile space caused the beach to evolve further landward, which is similar to the beach profile variation with wave height given by Liu et al. (Liu et al. 2019). Meanwhile, in view of the sandy beach elevation over beach profile changes, the sediment transport volume per unit width (V_s) was calculated to estimate the beach morphological development. Accordingly, it was found that larger pile space led to the increasing transported sediment volume (V_s/H^2), owing to the fact that the transmitted wave energy increased with the adjacent pile space increasing. Therefore, it is anticipated that the aforementioned sediment transport volume was less than the scenario without piles on a sloping sandy beach (i.e., the + inf in Fig. 13, which is denoted as the case in Section 4.1).

Fig. 11 Local scour depth around the piles ((a), (c), and (e) are the scour depth changes along the time at the front, side, and back of the most centered pile, respectively. (b), (d), and (f) are maximum scour depth changes under different S/D at the front, side, and back of the most centered pile, respectively.)

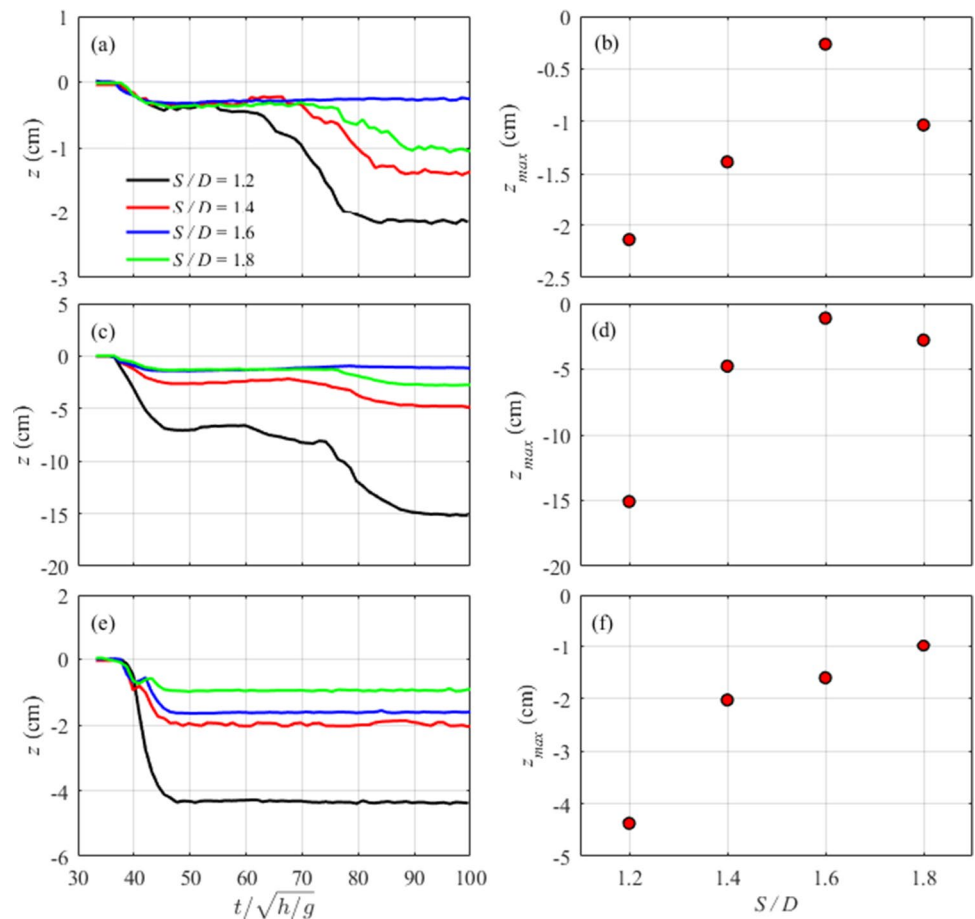
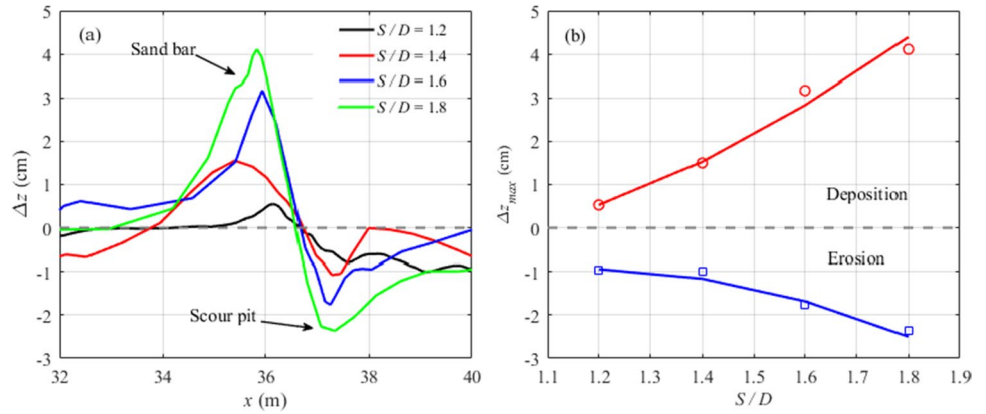


Fig. 12 Profile change of nearshore beach and the maximum scour depth (a) the profile change of nearshore beach under different S/D ; (b) relative maximum scour and deposition changes with different S/D



4.4 Analysis of long-term wave impacting

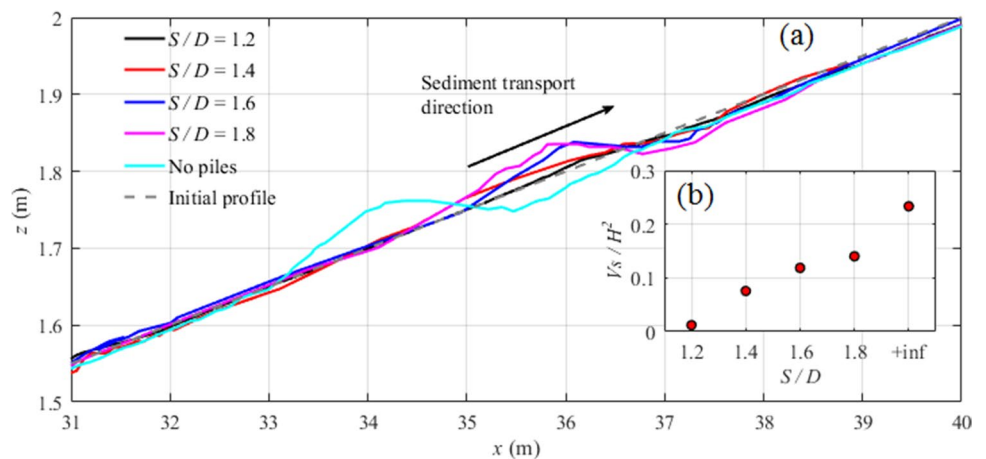
A long-term simulation using the wave, beach, and pile information provided by Reedijk and Markus (Reedijk and Muttray 2007) was performed to comprehend the role of pile rows in the evolution of sandy beaches in the real world. The beach slope is approximately 1:25, with an average beach grain size $d_{50} = 0.2$ mm. The pile diameter was 350 mm, and the center-to-center spacing is 70 mm. Near the location of the pile row, the significant wave height is approximately 1.5 m during the extreme atmosphere. Figure 14 shows the local beach evolution around the pile row after several waves. The local beach evolved into a deep scour hole under wave impact, and the erosion hole reached equilibrium after the fifth wave.

Figure 15 shows the beach profile evolution with and without pile rows after the impact of several waves. Evidently, significant erosion occurred around the waterline, and sand was transported along the offshore direction where a bar formed. The sandbar size increased as the wave number increased, while the sandbar center moved seaward. As the pile row clearly formed an obstacle for the sediment moving in the offshore direction, the erosion around the

waterline was reduced. Nevertheless, the obvious beach erosion around piles is found, and the scour depth was larger in the gap between adjacent piles where the maximum scour depth reached about 0.5 m for this wave condition. Overall, the observations of the present study conform with the report by the resort manager that the pile row not only reduced the tsunami impact but was also effective in trapping sediments during the tsunami event that struck South East Asia in December 2004 (Reedijk and Muttray 2007).

To the best of our knowledge, the scouring condition of a single pile in this area is necessary to determine the group of piles built on a coastal beach, and an empirical coefficient is used to amplify its influence to calculate the scour around the pile group. However, in contrast to the scour on the flat seabed, nearshore profile changes also need to be considered, apart from the local scour around the piles associated with the sandy beach in the design. Unfortunately, there are no references in the design manuals to comprehensively predict the local and nearshore scour during the interaction between the wave and the sandy beach. In the present study, we propose a numerical approach to resolve the aforementioned predicaments. Based on the current results, the nearshore scour scope and transported sediment volume decreased as S/D decreased,

Fig. 13 Nearshore beach evolution affected by the piles ((a) beach evolution under different S/D ; (b) transported sediment volume changes with different S/D)



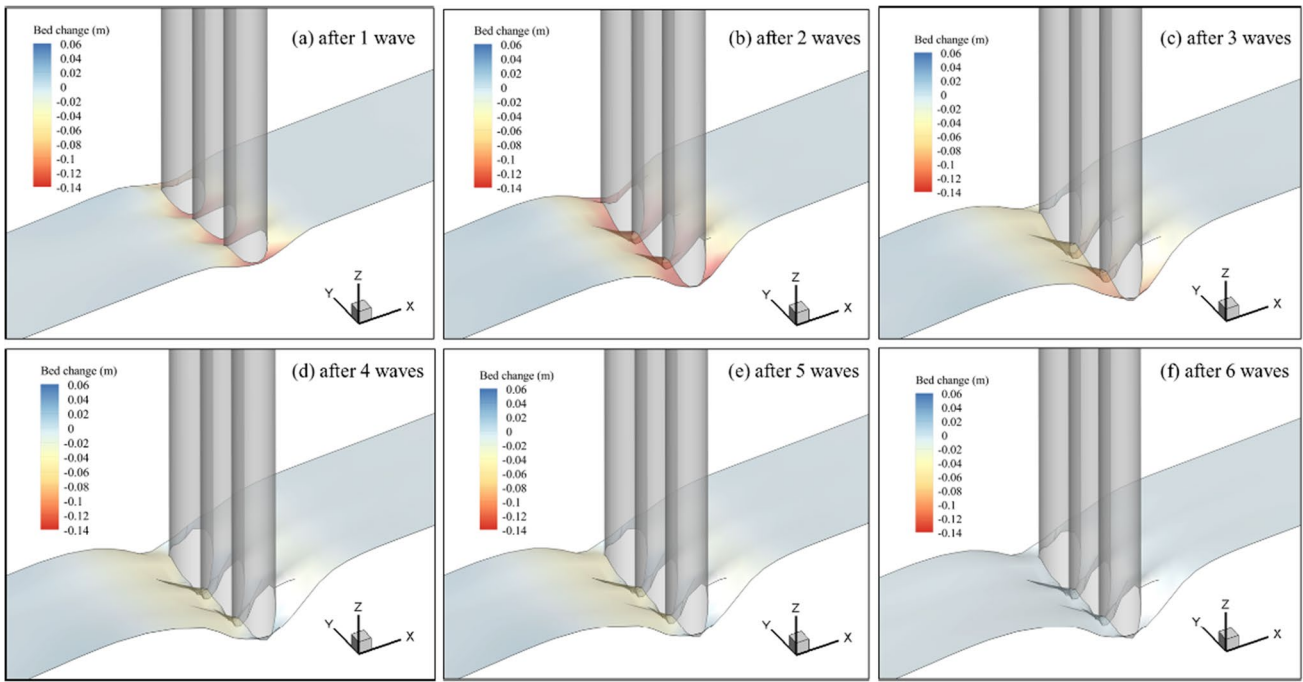
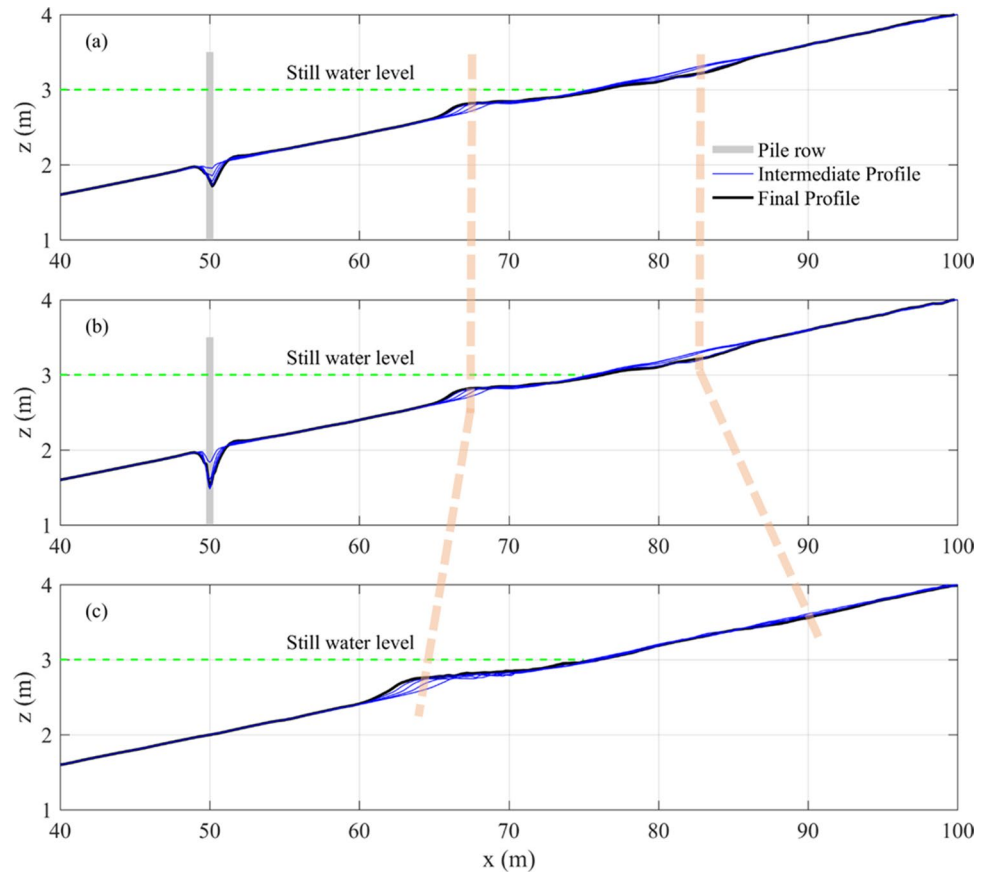


Fig. 14 Local 3D scour morphology around pile row after impacting of several waves (the color represents geomorphologic differences between adjacent waves)

Fig. 15 a Beach morphodynamic evolution along the monopile. **b** Beach morphodynamic evolution along the gap between adjacent piles. **c** Beach morphodynamic evolution without pile row



and in extreme cases, the pile row tended to have a seawall structure. However, the local scour around the piles increases, which may cause structural instability. Alternatively, based on existing scenarios, the S/D has been discussed preliminarily to weigh the potential hazards between local scour and nearshore scour. Moreover, we remarked that the S/D may also be affected by the beach slope and arrangement of the slotted piles; thus, the conclusions may be more or less different for other beaches with different pile configurations. Despite the aforementioned uncertainties, it is believed that the findings drawn from this study can significantly enhance our understanding of the efficiency of pile rows on sandy beaches in trapping sand, providing them as an engineering practice to prevent coastal communities and infrastructures from the devastating outcomes of extreme tsunamis.

5 Conclusions

A 3D coupled model of hydrodynamic and sediment transport based on OpenFOAM® was developed to explore the effect of the pile row breakwater on trapping sand and beach protection under waves. Typical formulae for the bedload and suspended load were employed to reproduce the sediment transport. The Exner equation was solved numerically, and the evolution of the bed morphology was updated closely once the resulting erosion and deposition were calculated. The robustness of the current model was validated by experimental data, and the results indicated that the numerical model was suitable for reproducing the hydrodynamics, local scour around the piles, and beach evolution.

The beach profile change under extreme waves, that is, tsunami waves, was first assessed, and it was found that beach scour was not obvious during wave run-up; however, the scour depth quickly increased owing to the rapid sheet downrush flow and hydraulic jump during wave drawdown. As the wave number increased, the sandbar size increased, and the sandbar center moved seaward. Subsequently, the effect of pile row structure on sandy beach evolution was analyzed, and the role of the space between adjacent piles was considered in detail. This shows that the construction of the pile row structure would change the wave propagation along the beach, resulting in the vortices around the piles experiencing serious fluctuations, such as deformation, stretching, and breaking, whose influence area on the leeside of the piles during run-up was less than that on the seaside during drawdown. Moreover, the vortex structures became more intense as S/D decreased during run-up, and they exhibited an opposite tendency during drawdown. When the S/D was less than 1.6, local scour decreased with the increasing of S/D . In contrast, when S/D increased from 1.6 to 1.8, the scour increased on the seaside of the piles and both side faces except the leeside. Meanwhile, the nearshore beach change moved landside under

the influence of the pile row, and the sediment transport volume and maximum scour depth decreased with the decrease in S/D ; however, they were smaller than in the case without piles. This demonstrated the effectiveness of pile rows in trapping sand and beach protection.

The real processes of the effect of pile row structure on sediment transport and sandy beach evolution tend to be more complicated than those modeled by existing simulations, such as the hydrodynamic and morphological processes near piles affected by currents and debris. Furthermore, different combinations of wave height, water depth, and beach slope are suggested, and an optimized S/D is proposed by weighing the hazards between local scour and nearshore scour.

Supplementary Information The online version contains supplementary material available at <https://doi.org/10.1007/s10236-022-01517-9>.

Acknowledgements Professor Changbo Jiang from Changsha University of Science & Technology and Professor Zhihe Chen from Sun Yet-Sen University and Xiujuan Wang are sincerely appreciated for their self-giving help.

Funding This study was supported financially by the Marine Economic Development (Marine six industries) Special Fund of Guangdong Province (grant no. GDNRC [2021]41), Guangdong Basic and Applied Basic Research Foundation (grant no. 2021A1515110428), and Applied Basic Research Programs of Guangzhou (grant nos. 201904010335 and 202102021286). The research was also financially supported by National Key R&D Program of China (grant no. 2021YFC3001000), National Natural Science Foundation of China (grant no. 51779280), and the Open Foundation of Key Laboratory of Water–Sediment Sciences and Water Disaster Prevention of Hunan Province (grant no. 2020SS02).

Data availability The data supporting the findings of this study are available with Xiaojian Liu upon a reasonable request.

Declarations

Conflict of interest The authors declare no competing interests.

References

- Allen JRL (1982) Simple models for the shape and symmetry of tidal sand waves: statically stable equilibrium forms. *Mar Geol* 48:31–49
- Arzani A, Gambaruto AM, Chen G, Shadden SC (2016) Lagrangian wall shear stress structures and near-wall transport in high-Schmidt-number aneurysmal flows. *J Fluid Mech* 790:158–172
- Babaeyan-Koopaei K, Ervine DA, Carling PA, Cao Z (2002) Velocity and turbulence measurements for two overbank flow events in River Severn. *J Hydraul Eng* 128:891–900
- Baykal C, Sumer BM, Fuhrman DR, Jacobsen NG, Fredsøe J (2017) Numerical simulation of scour and backfilling processes around a circular pile in waves. *Coastal Eng* 122:87–107
- Brørs B (1999) Numerical modeling of flow and scour at pipelines. *J Hydraul Eng* 125:511–523
- Engelund F, Fredsøe J (1976) A sediment transport model for straight alluvial channels. *Hydrol Res* 7:293–306

- FEMA (2008) Guidelines for design of structures for vertical evacuation from tsunamis. FEMA P646, Applied Technology Council, FEMA, Washington, DC
- Galperin B, Kantha LH, Hassid S, Rosati A (1988) A quasi-equilibrium turbulent energy model for geophysical flows. *J Atmos Sci* 45:55–62
- Higuera P, Lara JL, Losada IJ (2013) Realistic wave generation and active wave absorption for Navier-Stokes models: Application to OpenFOAM®. *Coastal Eng* 71:102–118
- Jacobsen NG, Fuhrman DR, Fredsøe J (2012) A wave generation toolbox for the open-source CFD library: OpenFoam®. *Int J Numer Methods Fluids* 70:1073–1088
- Jacobsen NG, Fredsøe J (2011) A full hydro- and morphodynamic description of breaker bar development. (Ph.D. thesis) Department of Mechanical Engineering, Technical University of Denmark
- Jasak H, Tuković Ž (2006) Automatic mesh motion for the unstructured finite volumemethod. *Transactions of FAMENA* 30(2):1–20
- Jeong J, Hussain F (1995) On the identification of a vortex. *J Fluid Mech* 285:69–94
- Jiang CB, Liu XJ, Yao Y, Deng B (2019) Numerical investigation of solitary wave interaction with a row of vertical slotted piles on a sloping beach. *Int J Nav Archit Ocean Eng* 11:530–541
- Kato F, Sato S, Yeh H (2000) Large-scale experiment on dynamic response of sand bed around a cylinder due to tsunami. In Proc. 27th Int Conf Coastal Eng, ASCE, Sydney, Australia 1848–1859
- Kato F, Tonkin S, Yeh H, Sato S, Torii K (2001) The grain-size effects on scour around a cylinder due to tsunami run-up. ITS 2001 Proc., Session 7. 7–24
- Khosronejad A, Kang S, Borazjani I, Sotiropoulos F (2011) Curvilinear immersed boundary method for simulating coupled flow and bed morphodynamic interactions due to sediment transport phenomena. *Adv Water Resour* 34:829–843
- Kobayashi N, Lawrence AR (2004) Cross-shore sediment transport under breaking solitary waves. *J Geoph Res* 109:1–13
- Kuswandi, Triatmadja R, Istiarto (2017) Simulation of scouring around a vertical cylinder due to tsunami. *Sci Tsunami Hazards* 36:59–69
- Kuswandi K, Triatmadja R, Istiarto I (2016) Velocity around a cylinder pile during scouring process due to tsunami. Congress of the Asia Pacific Division of the International Association for Hydro Environment Engineering and Research, At Colombo, Srilanka 20:1–8
- Larsen BE, Arbøll LK, Kristoffersen SF, Carstensen S, Fuhrman DR (2018) Experimental study of tsunami-induced scour around a monopile foundation. *Coastal Eng* 138:9–21
- Lee JJ, Skjelbreia JE, Raichlen F (1982) Measurement of velocities in solitary waves. *J Waterw Port Coast Ocean Div* 108:200–218
- Leveque RJ (2002) Finite volume methods for hyperbolic problems. Cambridge University Press, p 578
- Liang D, Cheng L, Li F (2005) Numerical modeling of flow and scour below a pipeline in currents: Part II. Scour Simulation. *Coastal Eng* 52:43–62
- Liu XF, García MH (2008) Three-dimensional numerical model with free water surface and mesh deformation for local sediment scour. *J Waterway Port Coastal Ocean Eng* 134:203–217
- Liu C, Liu XJ, Jiang CB, He Y, Deng B, Duan ZH, Wu ZY (2019) Numerical investigation of sediment transport of sandy beaches by a tsunami-like solitary wave based on Navier-Stokes equations. *J Offshore Mech Arct Eng* 141:1–13
- Liu XJ, Liu C, Zhu XW, He Y, Wang QS, Wu ZY (2020) 3D modeling and mechanism analysis of breaking wave-induced seabed scour around monopile. *Math Probl Eng* 1647640
- Mo W, Jensen A, Liu PL-F (2013) Plunging solitary wave and its interaction with a slender cylinder on a sloping beach. *Ocean Eng* 74:48–60
- Mori N, Takahashi T (2012) Nationwide post event survey and analysis of the 2011 Tohoku earthquake tsunami. *Coastal Eng J* 54:1250001
- Nielsen AW, Liu X, Sumer BM, Fredsøe J (2013) Flow and bed shear stresses in scour protections around a pile in a current. *Coastal Eng* 72:20–38
- Pan CH, Huang W (2012) Numerical Modeling of Tsunami Wave Run-Up and Effects on Sediment Scour around a Cylindrical Pier. *J Eng Mech* 138:1224–1235
- Qi WG, Gao FP (2014) Physical modeling of local scour development around a large-diameter monopile in combined waves and current. *Coastal Eng* 83:72–81
- Rambabu M, Rao SN, Sundar V (2003) Current-induced scour around a vertical pile in cohesive soil. *Ocean Eng* 30:893–920
- Reedijk B, Muttray M (2007) Pile row breakwaters at Langkawi, Malaysia, 10 years of beach development. Proc. Coastal Structures 2007, World Scientific, Singapore, pp 562–573
- Rijn LC (1984) Sediment transport, part II: suspended load transport. *J Hydraul Eng* 110:1613–1641
- Roeber V, Yamazaki Y, Heung KF (2010) Resonance and impact of the 2009 Samoa tsunami around Tutuila, American Samoa. *Geophys Res Lett* 37:L21604
- Saatcioglu M, Ghobarah A, Nistor I (2005) Reconnaissance report on the December 26, 2004 Sumatra earthquake and tsunami. Report Canadian Association for Earthquake Engineering, p 21
- Schlichting H (1979) Boundary-Layer Theory. 7th ed., McGraw-Hill, New York
- Soulsby RL, Whitehouse RJSW (1997) Threshold of sediment motion in coastal environments. Proceedings Pacific Coasts and Ports 1997 Conference, Christchurch, University of Canterbury, New Zealand, Wallingford, pp 149–154
- Sumer BM, Fredsøe J (2001) Scour around pile in combined waves and current. *J Hydraul Eng* 127:403–411
- Sumer BM, Hatipoglu F, Fredsøe J (2007) Wave scour around a pile in sand, medium dense, and dense silt. *J Waterway Port Coastal Ocean Eng* 133:14–27
- Takahashi S, Yoshiaki K, Takashi T (2011) Urgent survey for 2011 Great East Japan earthquake and tsunami disaster in ports and coasts-part I. Port and Airport Research Institute, Tokyo
- Tonkin S, Yeh H, Kato F, Sato S (2003) Tsunami scour around a cylinder. *J Fluid Mech* 496:165–192
- USGS (2010) Tsunami observations of tsunami impact. http://walrus.wr.usgs.gov/tsunami/sumatra05/Banda_Aceh/0638.html
- Xiao H, Huang W (2014) Three-dimensional numerical modeling of solitary wave breaking and force on a cylinder pile in a coastal surf zone. *J Fluid Mech* 141:1–13
- Yao Y, Tang Z, He F, Yuan W (2018) Numerical investigation of solitary wave interaction with double row of vertical slotted piles. *J Eng Mech* 144(1):04017147
- Zeng J, Constantinescu G, Weber L (2005) A fully 3D non-hydrostatic model for prediction of flow, sediment transport and bed morphology in open channels. Proc of the 31st IAHR Congress 1327–1338